New Fluorescent Tools for Watching Nanometer-Scale Conformational Changes of Single Molecules

Erdal Toprak[1] and Paul R. Selvin[1,2]

[1]Center for Biophysics and Computational Biology and [2]Physics Department, University of Illinois, Urbana-Champaign, Urbana, Illinois 61801; email: selvin@uiuc.edu, toprak@uiuc.edu

Annu. Rev. Biophys. Biomol. Struct. 2007. 36:349–69

First published online as a Review in Advance on February 13, 2007

The *Annual Review of Biophysics and Biomolecular Structure* is online at biophys.annualreviews.org

This article's doi: 10.1146/annurev.biophys.36.040306.132700

1056-8700/07/0609-0349$20.00

Key Words

fluorescence microscopy, motor proteins, measuring step sizes, motility mechanism

Abstract

Single-molecule biophysics has been serving biology for more than two decades. Fluorescence microscopy is one of the most commonly used tools to identify molecules of interest and to visualize biological events. Here we describe some of the most commonly used fluorescence imaging tools to measure nanoscale movements and the rotational dynamics of biomolecules.

Contents

MEASURING DISTANCES AND STUDYING ROTATIONAL DYNAMICS OF PROTEINS USING SINGLE-MOLECULE FLUORESENCE IMAGING TECHNIQUES

Single-Particle Tracking: Resolution and Orientation

It has been known for more than a century that the far-field diffraction limit of light is approximately $\lambda/2NA$, where λ is the wavelength and NA is the numerical aperture of the collecting lens. For a microscope, the maximum NA is <1.65. This means that two points, emitting in the visible wavelength, cannot be separated if they are closer than ~250 nm. If they are closer than this, the point spread function (PSF) of the two spots overlap into one; if farther than this, they are two well-resolved points. Recently, novel subdiffraction techniques have been introduced (12, 20, 46, 47) to achieve a resolution of <50 nm.

Other workers have focused on tracking of single particles. Here the far-field diffraction limit does not apply, and one can determine the position of an object with unlimited accuracy, although the amount of photons hitting the detector is limiting, as well as other sources of background (Equation 2). For example, Gelles et al. (17) used 1-μm latex beads with differential interference contrast microscopy, at 30 frames per second, and observed little molecular motors (kinesin) transport the beads with a precision of 1 to 2 nm. Sheets et al. (36) and Geerts et al. (16) used 30- to 40-nm colloidal gold particles, with similar temporal and spatial resolution, detected by bright-field microscopy. More recently, Thompson et al. (40) observed fluorescent beads with a precision of ~2 nm, and developed a simple but elegant theory of precise localization. Yildiz et al. (49) have discovered how to study single fluorophores attached to biomolecules of interest to achieve ~1.5 nm localization of the fluorophore's centroid, with a temporal resolution of 1 to 500 ms (22, 28, 49, 51).

Single-molecule biophysics comprises more than measuring step sizes and distances,

and there is a need for tools that measure the rotational movements of biomolecules. The existing tools for measuring rotational dynamics are usually based on the polarized characteristic of light. A fluorophore typically acts like a transition dipole moment, i.e., it has an excitation dipole and an emission dipole. Dickson and coworkers (2–4) showed that the shape of a fluorophore's image collected with a defocused lens depends on the dye's orientation. Goldman and colleagues (15) used total internal reflection (TIR) fluorescence microscopy with orthogonal polarizations to excite a single molecule in order to determine the dye's orientation when bound to myosin V molecules. Finally, we have utilized the work of both Dickson and colleagues and Goldman and colleagues to determine orientations and centroids using a technique called defocused orientation and positioning imaging (DOPI) (42), as well as polarization microscopy (39). The work is summarized here.

Fluorescence Imaging with One Nanometer Accuracy

Fluorescence imaging is widely used to study biological mechanisms. With classical fluorescence imaging methods, point-like fluorescent emitters (e.g., small organic dyes) cannot be localized to an accuracy better than ~250 nm because of the diffraction limit. However, better localization accuracy is necessary in order to study the mechanisms of biological molecules. For example, processive molecular motors such as myosin, kinesin, and dynein take discrete steps, which occur in the nanometer range (49–51). The study by Cheezum et al. (9) showed that fitting a two-dimensional (2D) Gaussian function to the emission pattern of a single fluorescent probe to obtain the centroid of a fluorescent probe is the best approach among other possible algorithms. Thompson et al. (40) later quantified all the parameters that affect the standard error of the mean (SEM) of the resulting fit and, using a charge-coupled device (CCD), demonstrated experimentally that fluorescent beads can be localized to ~2 nm. The main contributions to the SEM of a least-squares fit of the 2D Gaussian function arise from five sources: pixelation of the CCD camera, fluorescent background, readout noise from the CCD camera, number of photons, and photon noise. This approach was extensively developed by Yildiz et al. (49), and it was successfully applied to measure the step sizes of fluorescently labeled myosin V molecules. Yildiz et al. named the method fluorescence imaging with one nanometer accuracy (FIONA) (49). FIONA has been widely used by several groups to study the translocation of molecular motors or to measure small distances.

The emission intensity distribution [$I(x,y)$] of a fluorophore on the CCD imaging plane is fit to the following 2D Gaussian function in order to get the lateral position of the fluorophore in the specimen plane:

$$I(x,y) = I_{\text{background}} + A. \exp\left\{-1/2\left[\left(\frac{x-x_0}{s_x}\right)^2 + \left(\frac{y-y_0}{s_y}\right)^2\right]\right\}, \quad 1.$$

where x_0 and y_0 are the coordinates of the center, and s_x and s_y are the standard deviations of the distributions in each direction (**Figure 1*a***). The SEM ($\sigma^{\mu}_{x,y}$) of the 2D Gaussian function is

$$\sigma^{\mu}_{x,y} = \sqrt{\frac{s^2_{x,y}}{N_{\text{photons}}} + \frac{a^2}{12.N_{\text{photons}}} + \frac{8.\pi.s^4_{x,y}.b^2}{a^2.N_{\text{photons}}}}, \quad 2.$$

where N_{photons} is the number of the collected photons during one exposure period, a is the effective pixel size (a = CCD pixel size per magnification), and b is the background (40).

Possible Methods of Decreasing $\sigma^{\mu}_{x,y}$

It is possible to reduce the SEM to as low as 1 nm (or less) by increasing the number of collected photons (>10,000), decreasing

TIR: total internal reflection

DOPI: defocused orientation and position imaging

CCD: charge-coupled device

FIONA: fluorescence imaging with one nanometer accuracy

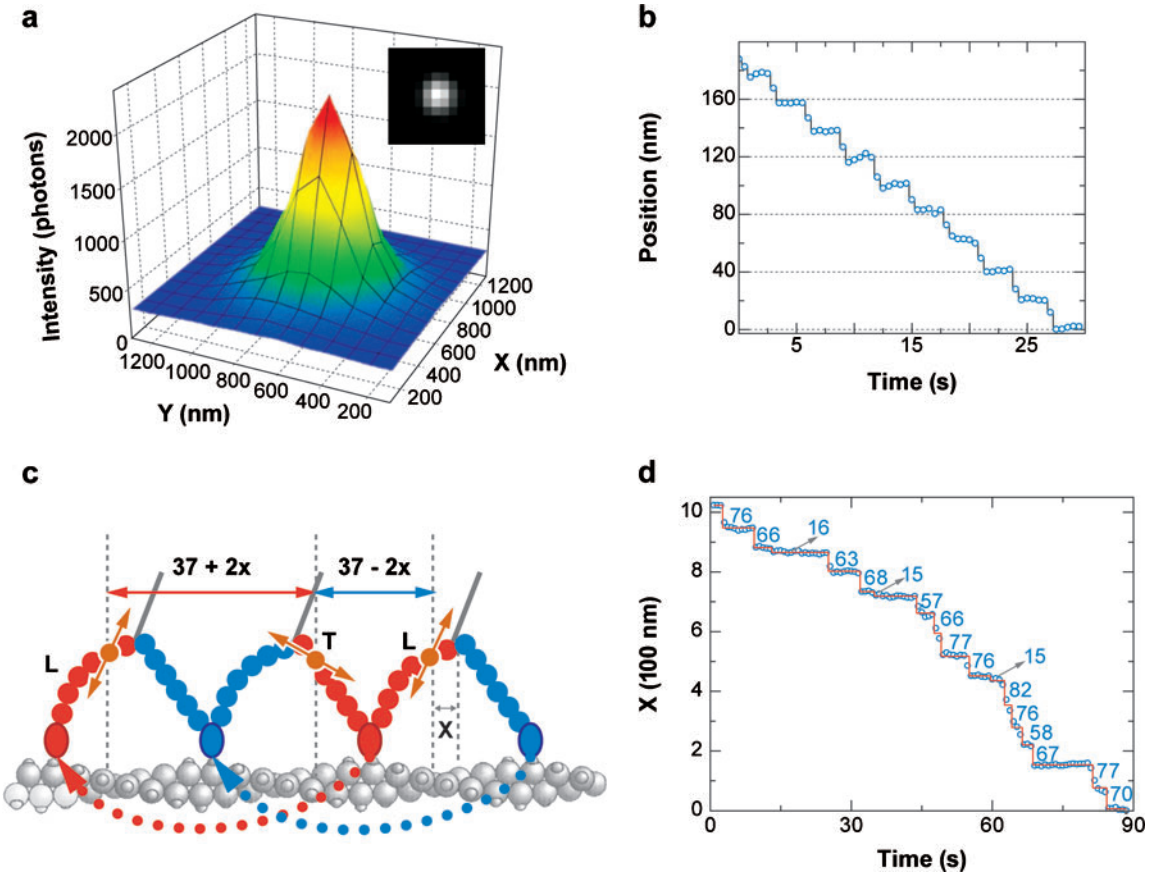

Figure 1

(*a*) The observed CCD image (*inset*) and the resulting point spread function of a fluorescent bead; the Gaussian fit is shown with wires. The standard error of the mean for the Gaussian fit is ~1.2 nm. (*b*) A fluorescent bead stuck to the coverslip was moved by 20-nm steps using a sample-holding piezo stage (Nano-Bio2®, Mad City Labs Inc.), and each frame was acquired for 0.5 s. (*c*) A cartoon illustration of two consecutive steps of a fluorescently labeled myosin V molecule with hand-over-hand fashion. Lever arms are blue and red. The motility direction is leftward. Only one of six IQ domains is labeled with a bifunctional rhodamine dye. The emission dipole of the dye is depicted by an orange, double-arrowed line. The center-of-mass displacement of myosin V is ~37 nm at each step. Therefore the measured step sizes are expected to alternate by $37 - 2x$ and $37 + 2x$ nm, where x is the projected distance between the dye and the center of mass of the myosin V. The lever arm is in a trailing state after short ($37 - 2x$) steps and in the leading state after long ($37 + 2x$) steps. The lever arm might be slightly curved in the leading state. (*d*) A sample displacement trajectory for a myosin V molecule. The average step size is ~76 nm, with a standard deviation of 9.8 nm. The short step size is hidden likely because of the dye location. The dye is likely to be close to the actin binding domain.

the fluorescence background and the size of the effective CCD pixels, or both. Objective-type TIR microscopy significantly reduces the background, and the high NA (1.40–1.65) oil-immersion objective lenses significantly increase the number of collected photons. Prism-type TIR is another method to increase the signal-to-noise ratio (SNR), despite its reduced photon collection efficiency. (We generally prefer objective-type TIR

because of the increasing collection efficiency.) Epifluorescence microscopy is also amenable to FIONA experiments, however, at the expense of a much higher background level compared with TIR imaging (49). A way in which to understand the necessary photon number and background level is to obtain a SNR of ~30 for the peak value of the PSF ($SNR = I_{peak}/(I_{peak} + b^2)^{0.5}$). The most straightforward way to achieve a higher SNR is to use longer exposure times during imaging. Another way of decreasing $\sigma^{\mu}_{x,y}$ is to decrease the pixel size. However, decreasing $\sigma^{\mu}_{x,y}$ by reducing both the effective pixel size and the background is not possible. The intensity decreases as a function of the magnification ($I \propto 1/M^2$, where M is the magnification), and this leads to an intrinsic background increase.

In summary, small pixels (<50 nm) may not be useful because they reduce the SNR and the observation area. Furthermore, large pixel sizes (>200 nm) are not useful because the PSF converges to a 2D delta function rather than to a 2D Gaussian function. A good way of selecting the right pixel size is to predict the full width at half maximum (FWHM ≈ 250 nm) of the emission distribution. An effective pixel size ranges from 30 to 50% of the FWHM, which corresponds to a value between ~80 and ~150 nm for the visible light. We typically choose either 86 or 100 nm for most of the single-molecule experiments.

Suppressing blinking events and increasing photostability of the dyes through the use of an enzymatic oxygen scavenging system and reducing agents are also essential for FIONA experiments (49). The exact reducing agents, including the manufacturers of the glucose oxidase and catalase, are necessary (49). Trolox is a promising reducing agent (31). Piezo stages can be useful for testing both the optical adequacy of the imaging system (SNR, stage drifts, etc.) and the fitting algorithm used. **Figure 1*b*** shows a trace of artificial 20-nm steps by using a piezoelectric stage.

FIONA Applied to Processive Cytoskeleton Motor Proteins

BR: bifunctional rhodamine

A number of different processive cytoskeleton proteins exist, including actin-dependent motors, such as myosins, in particular, myosin V and myosin VI, as well as microtubule-dependent motors, such as kinesins and dyneins. These molecular motors have been studied using single-molecule techniques for the past two decades, most often with optical traps, and their step sizes have been successfully measured (6, 24, 33, 34, 43). According to these experiments, myosin V has a ~37-nm step size and myosin VI has a ~30-nm step size. On the other hand, microtubule-dependent molecular motors, such as conventional kinesin, cytoplasmic dynein, and dimeric EG5, have ~8-nm step sizes. There is still not much known about the stepping mechanism of dynein. These experiments were performed using optical tweezers, in which a polystyrene microsphere was attached to the stalk of the motor protein and the center-of-mass displacements and the stall forces of these proteins were obtained. The center-of-mass movements, however, do not give any information about the dynamics of the individual motor domains of these proteins. Therefore it was not possible to distinguish between the two predicted walking models: inchworm versus hand-over-hand. Each of the proposed models makes testable predictions as to the motions of the protein during ATP-dependent translocation (49).

To address this mechanistic question, one light chain of a myosin V molecule was labeled with a bifunctional rhodamine (BR) or a cyanine 3 (Cy3) dye and an in vitro motility assay was performed at ~300 nM ATP (49). Because only one light chain of myosin V was labeled (**Figure 1*c***), ~37-nm steps were expected if the inchworm model was valid. However, alternating $37 - 2x$ (short) and $37 + 2x$ nm (long) steps were expected if the hand-over-hand model was valid, where x is the average distance between the center of

the myosin V and the dye projected on the specimen plane (**Figure 1*c***). Yildiz et al. (49) observed alternating long and short steps (74 – 0 nm, 52 – 23 nm, 44 – 30 nm), suggesting that myosin V was indeed walking hand-over-hand (**Figure 1*d***). Sakamoto et al. (35) determined that the length of the leg determined the step size and that the 74 – 0 nm steps were actually ~64 – 10 nm steps (39, 42). Furthermore, Yildiz et al. (51) showed that conventional kinesin moves hand-over-hand, and Ökten et al. (27) and Yildiz et al. (50) showed that myosin VI also moves via a hand-over-hand mechanism. Recently, Reck-Peterson et al. (32) showed strong evidence that cytoplasmic dynein also has a hand-over-hand stepping mechanism.

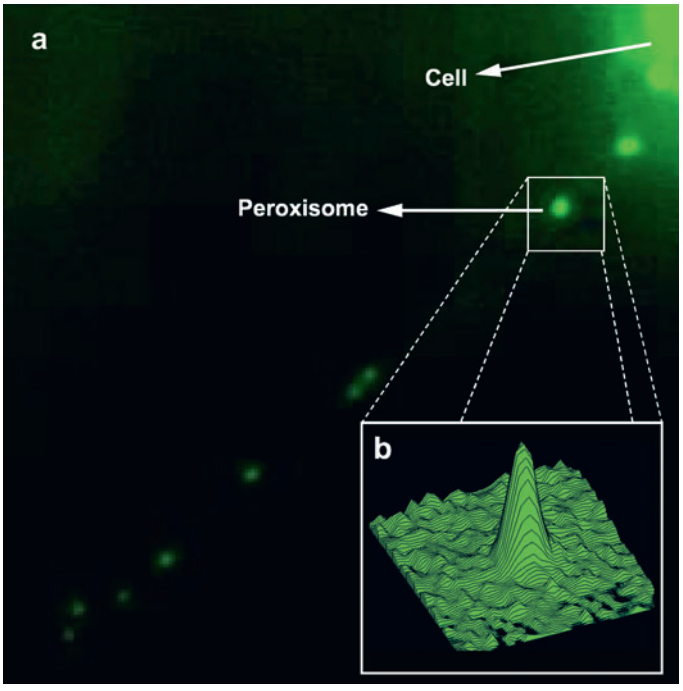

Figure 2

(*a*) The fluorescent image of an S2 *Drosophila* cell treated with cytochalasin D, which formed microtubule-containing long processes. Several peroxisomes are moving along the microtubules. The region of interest containing one of the peroxisomes is shown within the square. (*b*) The 3D plot of the fluorescent image of the peroxisome within the square. Imaging was done using an objective-type TIR setup.

In Vivo FIONA

Most motility experiments measuring the step sizes have been performed in vitro, because the experimental conditions can be controlled to reduce the effects of unknown parameters that exist within the cell such as high fluorescent background, nonuniform drag coefficients, complicated actin or microtubule geometries, and other interacting enzymes. The drawback to such in vitro experiments, however, is long sample preparation times. In vivo experiments on the other hand have the advantage of simpler sample preparation and the aforementioned difficulties can be handled through the use of clever experimental designs.

For example, Kural et al. (22) recently performed an in vivo experiment to study the motility mechanism of conventional kinesin and cytoplasmic dynein in *Drosophila* S2 cells, which expressed eGFP with a peroxisome-targeting sequence. Labeled peroxisomes consist of a large number of eGFP molecules depending on their size. Furthermore, the fluorescent background of the cell was reduced by using an objective-type TIR setup and the cells were chilled to ~10°C to slow down protein motion. To isolate peroxisome movement by kinesin and dynein movement and to eliminate the effect of actin, the authors treated the cells with cytochalasin D. Removing the actin content not only yielded pure microtubule-dependent motility, but also created linear tracks on which the organelles could move, since S2 cells tend to grow thin linear cell structures (called processes) filled with microtubules (**Figure 2*a***). The motility of the peroxisomes was recorded in the TIR volume on these linear tracks.

Kural et al. (22) could also determine whether the peroxisome was being moved by a kinesin (moving away from the nucleus) or by dynein (moving toward the nucleus). (In earlier experiments, while looking at peroxisomes within the cell body, without processes, it was not possible to determine definitely whether the peroxisomes were driven by

kinesin or dynein.) Kural et al. successfully measured the step sizes of kinesin (~8 nm) and dynein (~8 nm) with a temporal resolution of 1.1 ms and a position accuracy of ~1.5 nm (**Figure 2*b***).

Similar in vivo experiments were done by Nan et al. (26) and Toba et al. (41), who used quantum dots as probes to study cytoplasmic dynein and kinesin motility inside the cell. We should mention that the dynein experiments performed by different groups are not in absolute agreement on dynein step sizes and stall forces (22, 24, 26, 32, 41). The reason for these different observed step sizes and the stall forces is not yet apparent.

Pros and Cons of FIONA

FIONA has the great advantage of using wide-field illumination (usually a ~50 × ~50 μm area), whereby many molecules can be observed simultaneously. The covalent attachment of organic fluorophores does not adversely affect motor function (but this must always be tested) and furthermore does not impose significant additional load. The cost of an objective-type TIR setup is usually much cheaper than the cost of other optical designs (i.e., optical tweezers). A standard fluorescence microscope can be converted to a TIR microscope by using a laser line for the illumination and a high NA (>1.4) oil objective. Commercial TIR microscopes are also available.

Furthermore, FIONA does not need any special calibrations; rather, the only parameter needed is the effective pixel size, which can be easily obtained by knowing the real CCD pixel size and the magnification of the imaging optics. Currently, the time resolution of FIONA can be reduced to ~20 ms for single-fluorophore imaging (data not shown) and to submilliseconds for an object that contains several fluorophores or quantum dots (22, 26).

Brightness, especially for in vivo work and on single-molecule fluorophores, is a significant limitation. Photostability of the fluorophores is another major challenge for FIONA experiments. Optical probes such as quantum dots and gold nanoparticles, which last longer than conventional fluorophores, may provide attractive alternatives to the current suite of fluorescent dyes and fluorescent proteins (23, 25, 26, 40). Quantum dots are especially attractive candidates and they have been used by several groups for in vivo and in vitro studies (11). However, current obstacles to the use of quantum dots, such as low labeling efficiency, blinking, large effective size, nonuniform size and shape, and nonuniform excitation and emission characteristics, all require significant improvements (11, 26, 45).

Unlike optical or magnetic tweezers, FIONA does not apply force onto molecules. Therefore, combining force spectroscopy techniques such as optical and magnetic tweezers with FIONA will constitute a significant development. We are currently combining optical traps with FIONA.

Two-Color FIONA Imaging or SHREC

Conventional microscopy cannot resolve two molecules closer than ~250 nm, the far-file diffraction limit, also known as the Rayleigh limit. Fluorescence resonance energy transfer (FRET) can effectively measure distances between ~2 and ~10 nm. However, many conformational changes occur in the range of 10 to 250 nm, which is not accessible by conventional light microscopy or FRET. Therefore an alternative approach, such as differential labeling of particular sites of proteins, is required. In many cases, biological macromolecules provide sufficient reactivity such that two-color labeling can be achieved with a variety of organic and inorganic dyes.

A particularly powerful technique is two-color FIONA, also called single-molecule high-resolution colocalization (SHREC), developed by the Spudich group (10). This method relies on having two fluorophores that have sparse emission peaks, which are then imaged on the same CCD camera. Both dyes are excited by two separate laser lines and

FRET: fluorescence resonance energy transfer

SHREC: single-molecule high-resolution colocalization

the resulting emissions are split with the appropriate dichroic mirrors and emission filters. After obtaining the images of both fluorophores from the CCD, one can apply a mapping function to colocalize the dye positions. Usually two-color experiments have the difficulty of finding a sharp focal plane for both colors simultaneously because of the chromatic aberrations of the microscope objective. However, it is possible to use a meniscus lens to compensate for the focal plane difference due to the chromatic aberrations. (We use a commercial dual-view tube manufactured by Optical Insights, LLC for two-color imaging.)

Churchman et al. (10) colocalized Cy3 and Cy5 dyes, which were attached to two ends of a short DNA, and measured distances as small as 10 nm between the two. Furthermore, SHREC was used to measure the step size of myosin V, which was labeled with a Cy3 on one lever arm and a Cy5 on the other (10). Finally, A. Yildiz, Y.E. Goldman, and P.R. Selvin (unpublished results) used an approach similar to that used by Churchman et al. (10) to label myosin V with Cy3 and Cy5 and to measure the step sizes when myosin V was walking (**Figure 3**).

Two-color FIONA has also been performed with two different quantum dots, one on each head of the myosin V (45). One quantum dot had an emission peak at 565 nm, and the other had an emission peak at 655 nm. Quantum dots are handy for two-color experiments because different quantum dots can be excited simultaneously with the same excitation source. Warshaw et al. (45) measured the distance between the motor domains to be ~36 nm and a step size of ~72 nm when the motor domain goes from the trailing state to leading state. One problem was that only a small percentage (~3%) of myosin V walked while having two quantum dots (D.M. Warshaw, personal communication).

Although these recent experiments did not provide any new information regarding the myosin V motility mechanism, they did provide a new, general method for studying molecular motors. This technology enables researchers to observe the dynamics of different sites of a molecule at the same time. FRET is limited to 2 to 8 nm, while SHREC is

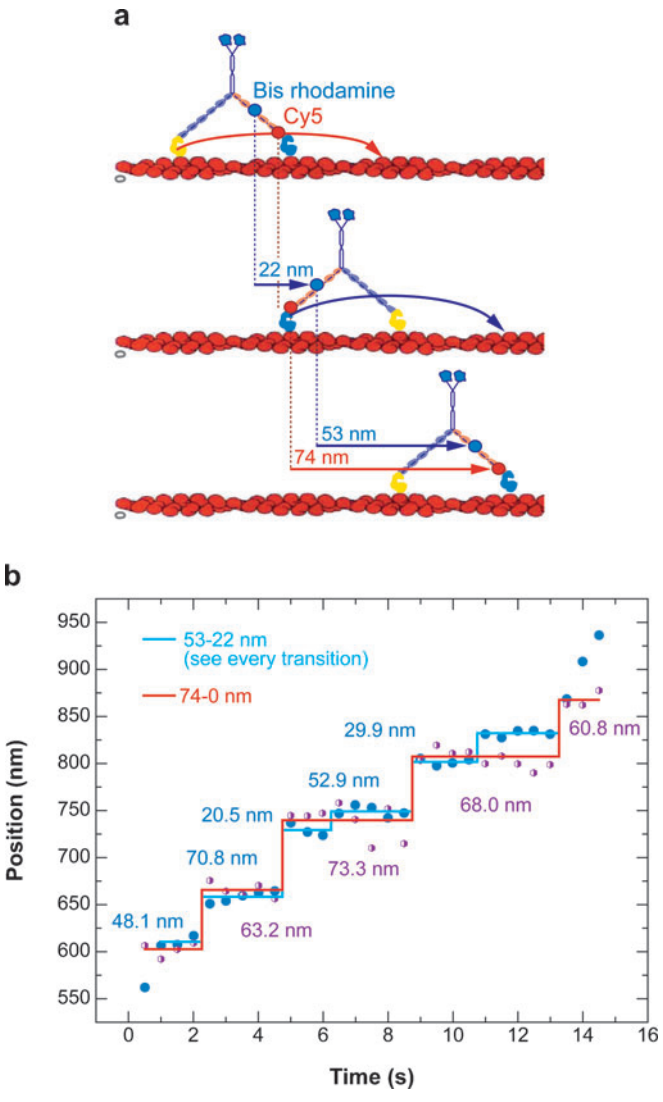

Figure 3

(*a*) A sample motility trace for a myosin V molecule labeled with a bifunctional rhodamine (BR, *blue circle*) and a cyanine 5 (Cy5, *red circle*) dye. (*b*) The estimated dye–myosin V geometry. The Cy5 dye (*purple circles* and *red fit line*) shows alternating ~74 – 0 nm steps; therefore it is likely located very close to the actin binding domain. However, BR dye (*blue circles* and *blue fit line*) shows alternating ~52 – 23 nm steps; therefore it is possibly located on another IQ domain that is farther from the actin binding domain. Both dyes are on the same lever arm.

capable of measuring 8 nm and longer. One downside to the technique is that, so far, relatively few available dye pairs have the requisite photostability. Cy3 (or rhodamine) and Cy5 are nearly optimal existing organic dye pairs for SHREC experiments. We suspect that with the addition of Trolox, an effective photostabilizer for Cy3 and Cy5, SHREC will be suitable for more applications (31).

Measuring Small Distances Using SHRImP

Single-molecule high-resolution imaging with photobleaching (SHRImP) is a technique introduced by Gordon et al. (18) to measure small distances (>10 nm) between identical immobile fluorophores. SHRImP is a method of obtaining the individual centroid for each of the two closely spaced fluorophores, which are otherwise not separately resolvable.

Briefly, a spot on the CCD camera that photobleaches in two steps is identified (**Figure 4*a***). Once the first dye has bleached, the resulting image—the second fluorophore—is fit to a single 2D Gaussian function. To obtain the position of the first dye, the image after photobleaching of the second dye is subtracted from the image before photobleaching of the first dye. This image is then also fit to a single 2D Gaussian function (**Figure 4*b***). The difference in centroids of the two dyes is then the distance between the two fluorophores. Gordon et al. (18) successfully measured the distance between two Cy3 dyes that are attached to short segments of DNA (>10 nm).

SHRImP is also used to measure the interhead distances of myosin VI molecules bound to actin filaments. Using an eGFP-myosin VI fusion protein, Balci et al. (1) determined that the average interhead distance is ~29 nm when myosin VI was bound to actin. As mentioned above, SHRImP is useful for immobilized molecules, unlike SHREC. However, SHRImP is easier to apply. For example, one does not need to find a reliable, different colored dye pair, and efficient labeling is not as difficult as multicolor labeling. Inherent optical problems such as chromatic aberrations do not occur with SHRImP.

SHRImP: single-molecule high-resolution imaging with photobleaching

STUDYING ROTATIONAL DYNAMICS WITH SINGLE-MOLECULE FLUORESCENCE TECHNIQUES

Single-molecule biophysics comprises more than simply measuring the step sizes of molecular motors. For instance, many proteins such as F1-F_0-ATPase (48), nonprocessive molecular motors, and ion channels do not move processively, but rotate. Here we describe some of the techniques that can be used with wide-field illumination and for studying the orientation (as well as the translation) of single biological molecules.

Taking Advantage of the Polarization of Light

The 3D orientations of the fluorophores that have linearly polarized excitation and emission dipoles can be detected by taking advantage of the polarized characteristic of (incident and/or emitted) light. Therefore one can study rotational dynamics of biological molecules by attaching a fluorophore so that it is rigid and does not undergo rotations independent of the target molecule's rotations.

Polarization modulation was applied to single fluorophores by Ha et al. (19). The dyes immobilized on the surface were excited with polarized light and the polarization was continuously modulated (**Figure 5*a***). The excitation yield varied with respect to the angle between the excitation dipole of the fluorophore and the polarization of the excitation laser. The resulting intensity profile of the fluorophore can be fit to a quadratic cosine function, and the in-plane angle (the angle around the optical axis) of the fluorophore can be extracted (**Figure 5*b***). However, polarization modulation is not amenable to dynamic systems unless the modulation and exposure

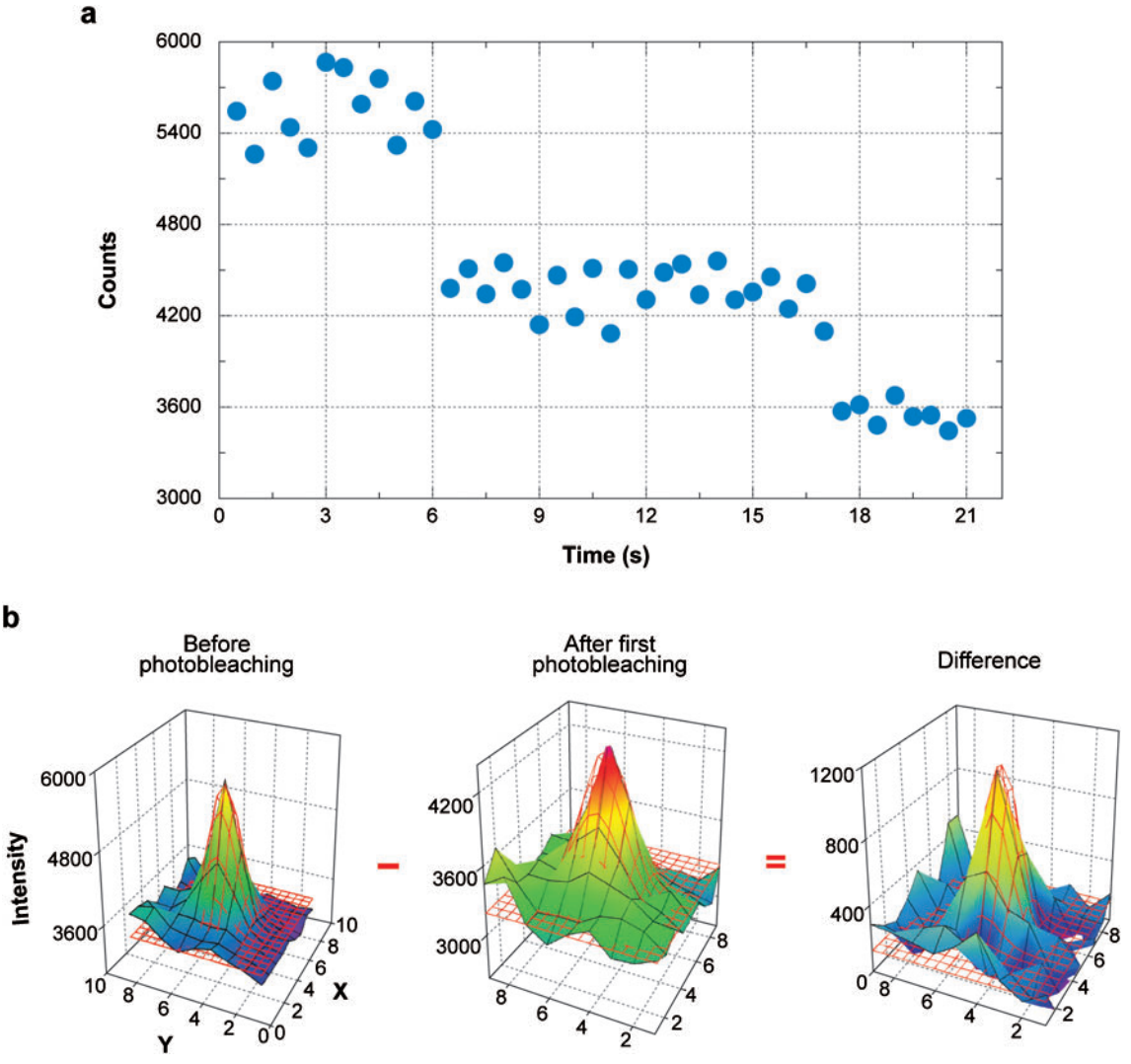

Figure 4

(*a*) A dimeric myosin VI molecule is labeled with GFP molecules on the motor domain and excited with a 488-nm laser line. Myosin VI was attached to the actin filament during the imaging time. The intensity profile shows the two-step photobleaching events of the GFP molecules. (*b*) The point spread function of the two GFP molecules before and after the first photobleaching event (*left to right*). The difference of these two functions gives the approximate point spread function of the first photobleached GFP molecule. Therefore it can be used to find the centroid of the first photobleached GFP. The remaining point spread function after the first photobleaching event is used to find the centroid of the second photobleached GFP molecule.

speed are high enough compared with the rotational dynamics of the target molecule.

An alternative way of finding the in-plane angles is to fix the excitation dipole and record the intensity fluctuations caused by rotations (38). However, it is usually difficult to relate the fluctuations and the rotations using only one excitation laser beam. Therefore it is essential to use two carefully calibrated beams that have orthogonal polarizations. Both

approaches have generic angular and dipolar degeneracy problems and do not give any out-of-plane angle information. A similar approach was used by Kinosita and coworkers (21) to obtain out-of-plane angles in order to measure the axial rotations of the actin filaments caused by myosin molecules. The idea is based on splitting the emission coming from a dye into vertical and horizontal polarizations and calculating the out-of-plane angles. However, both of the approaches need further information to get the full 3D orientations for single molecules, which was performed by Forkey et al. (13–15).

Forkey et al. (15) cleverly combined the approaches of both Ha et al. (19) and Kinosita et al. (21) to get the full 3D orientation information. They used an advanced prism-type TIR setup to excite the BR molecules. Their TIR setup included two orthogonal incident beams. Each of the beam's polarization was switching between horizontal and vertical polarizations, such that they had four different excitation beams (first beam vertical polarization, first beam horizontal polarization, second beam vertical polarization, and second beam horizontal polarization). This approach has the advantage of creating evanescent fields using TIR that are in x, y, and z directions, depending on the excitation laser's incident angle and the polarization of the incident excitation laser. They also split the emission light with respect to the polarization, and each of the split emission lines was recorded with avalanche photo diodes (APDs). So for each cycle of excitation they had four excitation lines and two emission lines, resulting in eight different combinations. In this way they obtained the 3D orientation of a single fluorophore. This method, also called single-molecule fluorescence polarization microscopy (SMFP), detects only one molecule at a time because APDs are used for detection. But fast CCD cameras may be used instead, thus allowing more molecules to be observed simultaneously.

In addition to this technical improvement, Forkey et al. (15) designed a novel experiment. They labeled myosin V molecules with BR dyes and observed the 3D rotational dynamics of myosin V molecules when they were walking along actin filaments. The authors also used an actin-based coordinate system for unambiguous analysis. They reported that the probe attached to the lever arm had two well-defined angles with respect to the actin filament. On average this angular change was ~40°, and Forkey et al. also reported that almost half of the myosin V molecules were moving but not undergoing

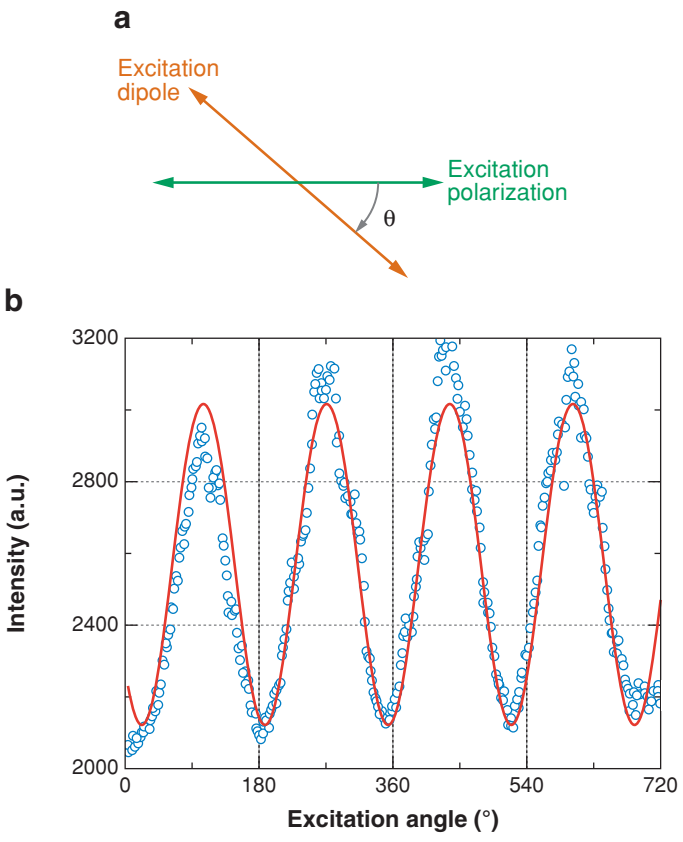

Figure 5

(*a*) The simplified geometry of the polarization modulation method. A frozen DiI molecule was excited by a linearly polarized 532-nm excitation laser. The excitation laser's polarization was continuously modulated by a half-wave plate mounted on a motorized rotary stage. (*b*) The resulting emission intensity of a DiI molecule that is excited as described above. The intensity profile can be fit to a quadratic cosine function ($I \sim A + B.\cos^2(\Phi_{excitation} - \Phi_{dipole})$). Intensity is maximum when $\Phi_{excitation} = \Phi_{dipole}$ or $\Phi_{excitation} = \pi + \Phi_{dipole}$ because of dipolar degeneracy.

APD: avalanche photo diode

SMFP: single-molecule fluorescence polarization microscopy

CaM: calmodulin

any rotational changes. However, this angular change of ~40° and the existence of nontilting myosin molecules were not consistent with the electron microscopy images (8, 44). The reason for this inconsistency, as explained by Forkey et al., was the fourfold angular degeneracy of the SMFP and the inherent twofold degeneracy of the dipoles. The angular degeneracy of SMFP can be reduced twofold by making extra polarization measurements (30).

Combining FIONA and Polarization Studies

SMFP is a powerful technique used for investigating rotational dynamics. However, because the emitted photons are detected by APDs, this method cannot report on translational movements as do FIONA and optical tweezers. On the other hand, FIONA has no capability to measure specific dye orientations. Achieving simultaneous localization and rotational dynamics data therefore requires combining SMFP with a position measurement technique. Syed et al. (39) successfully combined polarization studies with FIONA to study the translational and rotational dynamics of myosin V. Myosin V samples labeled on the light chain with a BR molecule were excited by switching between two orthogonal excitation lasers with the same polarization, which provided the ability to track the intensity fluctuations caused by reorientations of the dye and to measure precisely the motility of myosin V molecules at the same time. Unlike SMFP this method does not aim to get full 3D orientation information, rather it tracks qualitative intensity changes caused by lever arm reorientations (**Figure 6**). The BR molecule in this study was attached to the myosin by two bonds to minimize the thermal rotations of the dye. The exposure time for the experiments was either 500 or 150 ms and the positional accuracy was ~2 nm.

Previous in vitro myosin V experiments proposed a model in which the lever arm of myosin V was bent instead of straight. Snyder et al. (37) measured the step sizes of myosin V by labeling one of the motor domains with an eGFP molecule, and they observed alternating 74 – 0 nm steps, as expected. Surprisingly the step sizes measured by Yildiz et al. (49) for the myosin V labeled on one of its six calmodulins (CaMs) were 74 – 0 nm, 52 – 23 nm, and 44 – 30 nm depending on the dye location on the lever arm. The observation of 74 – 0 nm steps even when the dye was on the lever arm suggests a bent lever arm model (37). By combining FIONA with polarization measurements, Syed et al. (39) found that the 74 – 0 nm steps originally observed by Yildiz et al. were in fact 64 – 10 nm steps after using the qualitative information from intensity fluctuations due to lever arm reorientations.

Another interesting observation was the occurrence of ATP-dependent lever arm reorientations without any lateral movements. Combining FIONA with polarization methods is an excellent example of how monitoring multiple observables simultaneously can yield additional information not provided by either technique on its own.

Removing Angular Degeneracies Using Defocused Orientations and Position Imaging

Conventional microscopy techniques, which observe the specimen in the sharp focal plane, generally cannot report on the 3D orientations of the fluorophores. However, if the sample is deliberately moved away from the sharp focus by a specific distance (depending on the optical parameters), 3D orientations of the fluorophores can be found without any angular degeneracy (2, 3, 7, 42).

The defocused CCD image of a single fluorescent molecule is a combination of lobes and fringes depending on the orientation of the fluorophore (**Figure 7*a***). This method was first introduced by Dickson and coworkers (2, 3) and the complete description of the electrodynamics behind DOPI has been detailed elsewhere (2, 3, 7). In brief, the image of the single fluorophore is taken in

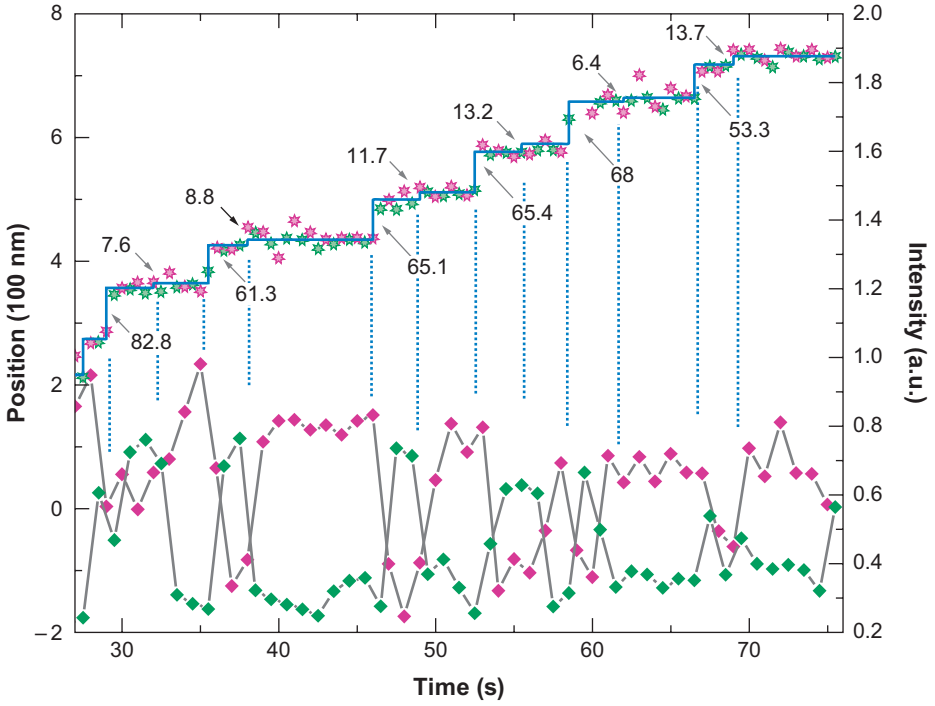

Figure 6

A myosin V molecule that has a bifunctional rhodamine on the lever arm was excited by alternating between two orthogonally polarized laser lines. The intensity fluctuations due to dye reorientations are observed (*green and pink diamonds*). The displacement trajectory (*pink and green stars*) was analyzed using the intensity information as the indication of the existence of a step. Therefore even statistically insignificant events are better resolved. This trace is shown in alternating ~64 – 10 nm steps.

a plane where the different light rays have not converged into a single focus. The resulting emission pattern of the single fluorophore on the CCD depends on Θ (the axial angle between dipole axis and optical axis), Φ (the azimuthal angle around optical axis), and δz (the defocusing amount from the focal plane) (**Figure 7*a***). Using a pattern-match analysis technique, Patra & Enderlein (29) calculated Θ, Φ, and the lateral position of the fluorophore. DOPI can detect the 3D orientations with ~10–15° uncertainty and lateral position with ~15 nm accuracy when the exposure time is 0.6 to 0.8 s (for a rhodamine molecule, ~3 mWatt excitation power with objective-type TIR illumination).

It is difficult to perform control experiments to test the angular accuracy of DOPI; therefore computer simulations are used to test the analysis algorithm. Perfect theoretical defocused images were computer generated and Poissonian noise was added to each pixel of the image. The total number of photons, background level, pixel size, and other optical parameters were all chosen according to our experimental setups and results, which were generally obtained (42). The fit results never deviated more than 5° when using the algorithm described by Patra & Enderlein (29). These simulations also showed that the sensitivity of DOPI for in-plane angles is higher when the out-of-plane angle of the dipole

is larger (i.e., more parallel to the specimen plane) (**Figure 7*b*,*c***). DOPI has no degeneracy in measuring the orientation of the dipole axis within any preselected hemisphere, but the bidirectional symmetry of the optical dipoles still presents an ambiguity between (Θ, Φ) and ($180^\circ - \Theta$, $\Phi + 180^\circ$) for any dipole.

An objective-type TIR setup was used to excite molecules, and the excitation laser was circularly polarized to excite all the dyes with maximum efficiency regardless of dye orientations. Choosing the right objective and the right effective pixel size is essential to observe defocused images. We used an infinity-corrected 100X 1.45NA oil objective (Olympus) and a 1.6X magnification unit to collect more photons and have a proper effective pixel size (total magnification was 160X, resulting in a 100-nm effective pixel size). Having pixel sizes smaller than 100 nm is possible, but increasing magnification decreases the intensity of the fluorophore dramatically. We started our experiments by looking at DiI molecules that were either dissolved in a polymer (methyl methacrylate or poly vinyl alcohol) or methanol. The dyes (~10 nM) were spin coated (3000 rpm for 30 s) on a precleaned coverslip (0.17-mm thickness) and then dried in an oven at 100°C for 1 min. For this setup and the emission wavelength (575 nm for BR), the optimal defocusing amount was ~500 nm. It is essential that the bond between the dye and the target molecule is rigid. We did not see any useful defocused patterns for Cy3 dyes that were attached to DNA with a single bond. The defocusing of the sample was done using a sample-holding piezoelectric stage (Mad City Labs Inc.). (It is not essential to start these experiments with a piezo stage; one can easily do the preliminary experiments by manually adjusting the focusing knob of the microscope.) By these experiments we optimized our imaging and excitation optics to ensure that we did not have any severe aberrations that could adversely affect our experiments.

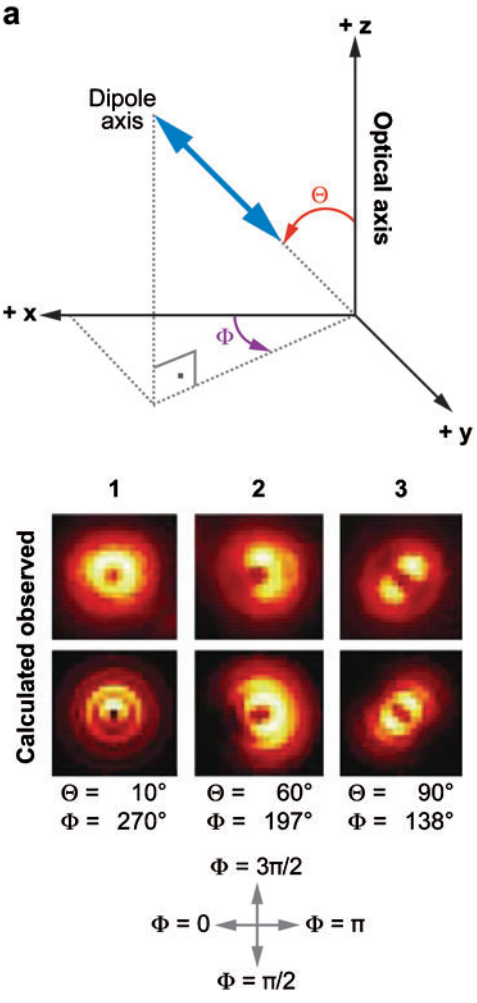

Figure 7

(*a*) The spherical coordinate system used in our calculations. Θ is the out-of-plane angle and Φ is the in-plane angle. (*b*) We tested the precision of our fitting algorithm by creating theoretical defocused images; the optical parameters, signal, and noise level were chosen according to our experimental setup. For a fixed in-plane angle we generated images with 3° Θ increments, and we fitted those images to theoretical patterns. The deviations of the Θ from Θ_{fit} are plotted against Θ values. These deviations are usually less than 2° (as shown). (*c*) The same procedure in panel *b* is repeated for in-plane angles Φ. For fixed Θ values (15°, 30°, 45°, 60°, 75°, 90°) we calculated average deviations of Φ from Φ_{fit} as a function of Θ values. The sensitivity of our algorithm for in-plane angle is enhanced when the dipole is more parallel to the surface.

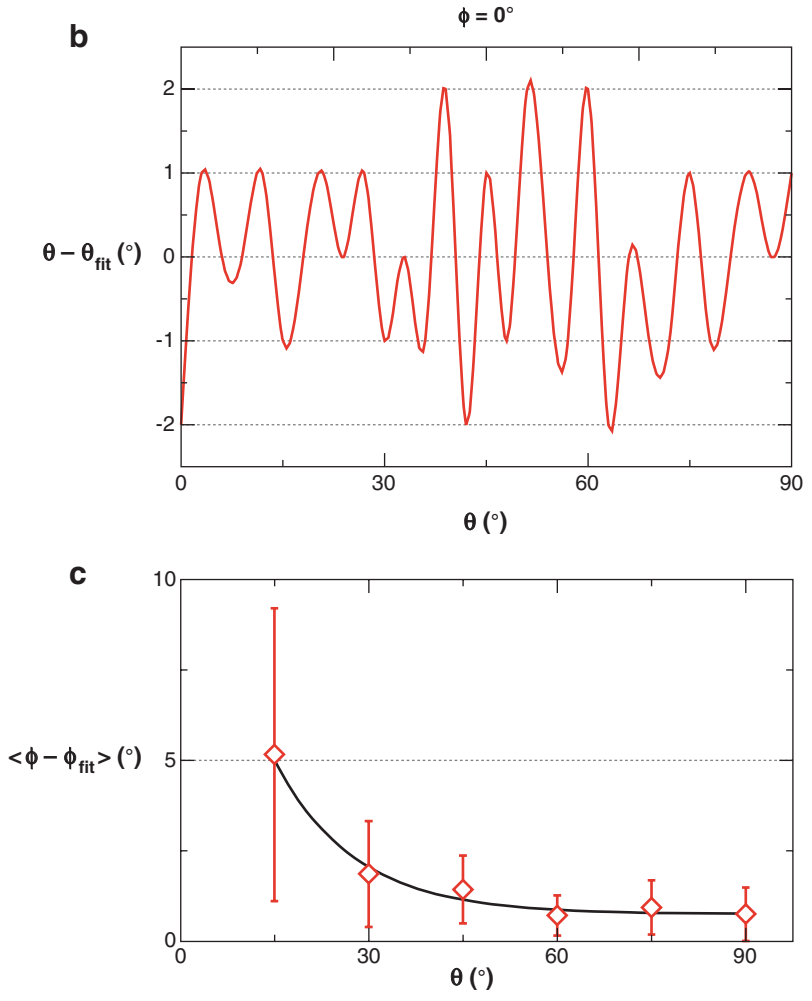

Figure 7
(*Continued*)

Studying Lever Arm Dynamics of Myosin V with DOPI

Evidence from previous studies (15, 44) indicates that the lever arm of myosin V has two well-defined states (trailing and leading) during ATP-dependent translocation and therefore was a perfect choice to demonstrate the capabilities of DOPI for biological studies. We labeled one of the six CaMs of myosin V with a BR. The orientation of the dye's dipole with respect to the lever arm is ~40°. However, the azimuthal angle of the dipole around the lever arm is not known. Also there was evidence that each CaM had a different orientation depending on its location on the lever arm. All these variables made using the lab coordinate frame unsuitable for an unambiguous analysis. Instead we used an actin-based coordinate system (**Figure 8*a***) to map everything on the actin frame (15). We defined two angles, α (the azimuthal angle around the actin) and β (the axial angle with respect to the actin filament).

We captured defocused images using exposure times between 0.6 and 0.8 s in the presence of ~300 nM ATP. The exposure time, ATP concentration, and excitation laser

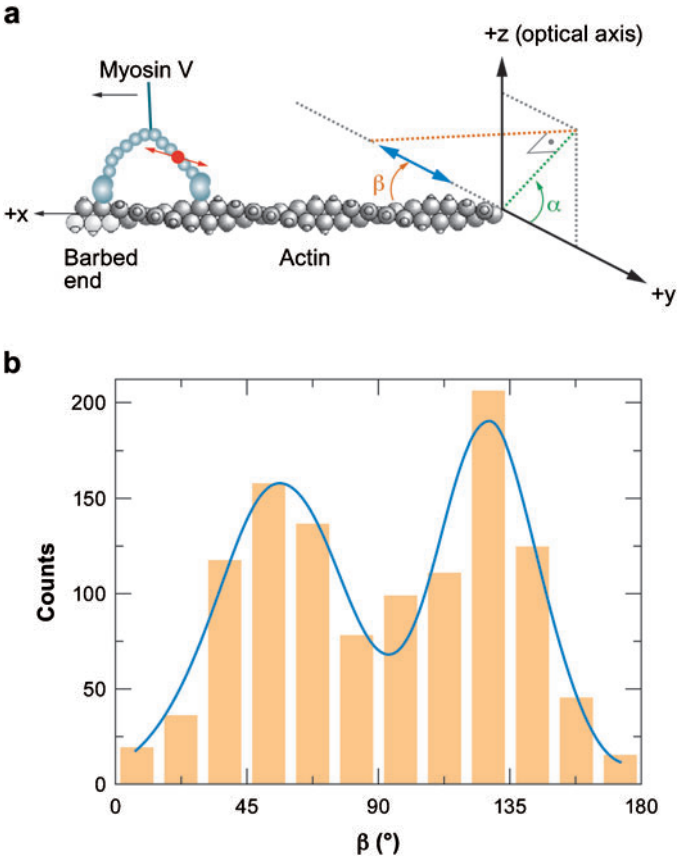

Figure 8

(*a*) The actin-based coordinate system adapted from Forkey et al. (15). This coordinate system is used for a less ambiguous analysis. α is the azimuthal angle between the dipole axis around the actin, whereas β is the axial angle with respect to the actin filament. (Also see **Figure 1*c*** and **Figure 3*a*.**) (*b*) The histogram of observed β angles while myosin V molecules were walking along the actin. The mean angles are 57° and 128° for the trailing and leading lever arms, respectively. (*c*) A sample trace of a myosin V molecule that was imaged by switching between focused and defocused imaging. The exposure time is 0.66 s per frame. We have captured repeated cycles of five consecutive defocused images and three consecutive focused images. The sample is moved away from the best focus by 500 nm. Blue circles are the raw position data analyzed by FIONA, and black lines are the averaged position within each dwelling period. Red diamonds are raw β values analyzed by DOPI and red lines are the dwell-averaged β values. Green triangles are raw α values and green lines are the dwell-averaged α values. The patterns above the graph are representative defocused images for each dwell time and the corresponding theoretically calculated patterns. (*d*) A sample trace of a myosin V molecule that was imaged by pure defocused imaging (DOPI). The exposure time is 0.75 s and the sample is moved away from the focus by 500 nm.

power (~3 mWatts measured before the objective) were optimized to capture four to five frames for each dwelling period of myosin V. Every myosin molecule that moved underwent the expected lever arm swing. This finding contradicts the results reported by Forkey et al. (15). We observed 65 molecules (which walked on a linear track, sparse enough for analysis, and moved processively for many steps), all of which showed well-defined lever arm rotations (**Figure 8*b***). The average β changes were ~71°, which were consistent with electron microscopy results (44). We observed ~27° azimuthal back-and-forth rotations (α changes) around the actin for almost 90% of the molecules. These rotations were correlated, or anticorrelated, with lever arm tiltings with respect to the actin (β changes).

However, the position accuracy of DOPI was usually not enough to measure step sizes at the same time. We measured the step sizes of myosin V by using a simple trick to take advantage of FIONA. By using a synchronized CCD and a piezo stage, we switched between focused and defocused imaging to get 3D orientations and accurate position data (**Figure 8*c*,*d***). These measurements (for 32 molecules) confirmed that all lever arm tiltings are synchronized with stepping events at our time resolution. Accurate step size information also allowed us to distinguish trailing states from leading states of the lever arm, because the lever arm is in the leading state

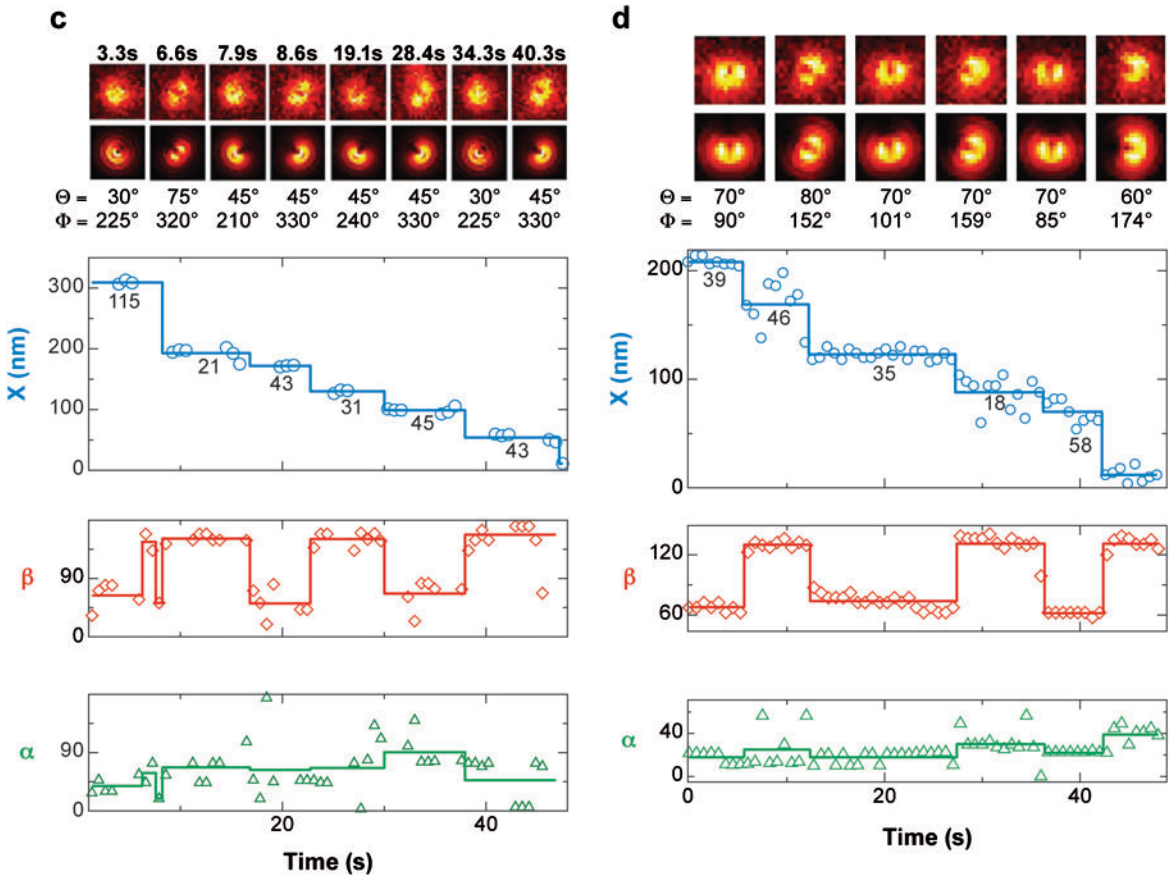

Figure 8

(*Continued*)

after long steps ($37 + 2x$ nm) and in the trailing state after short steps ($37 - 2x$ nm). We concluded that the average dipole angle with respect to the actin (β) was ~57° for the trailing lever arm and ~128° for the leading lever arm (**Figure 8*b***) for the 97 molecules and 1151 tilting events.

CONCLUSIONS AND FUTURE DIRECTIONS

The capabilities of modern imaging tools have shed light on biology since the invention of microscopes. Fluorescence spectroscopy and conventional microscopy still need much development, both in vitro and particularly in vivo. The inherent limitations of microscopy, such as the diffraction limit and the photostability problems of organic dyes and autofluorescent proteins, are still valid. Recent studies by several groups are pushing the diffraction limit to bring the optical resolution down to the nanometer range, although there is still room for improvement to extend the applications of the proposed methods (5, 20). These new imaging tools and future imaging tools will likely bring their own questions resulting from their high-resolution observations. Hopefully, these studies and the existing microscopy tools will be applicable for studying live organisms and used for medical purposes.

SUMMARY POINTS

1. Fluorophores can be localized within 1 to 2 nm accuracy using FIONA.
2. The translocation dynamics of biological molecules can be studied accurately by using fluorescence microscopy.
3. Single-molecule fluorescent techniques such as SHREC and SHRImP can be used to measure distances that cannot be measured with FRET.
4. Single-molecule fluorescent techniques such as DOPI and fluorescence polarization microscopy can be used to study the rotational dynamics of biological molecules.

ACKNOWLEDGMENTS

This work was supported by NIH grants AR44420 and GM068625. We thank Dr. Tyler Lougheed for his careful proofreading and suggestions on the text. We also thank Comert Kural, Hamza Balci, Sheyum Syed, and Ahmet Yildiz for generously sharing their original data for this review paper.

LITERATURE CITED

1. Balci H, Ha T, Sweeney HL, Selvin PR. 2005. Interhead distance measurements in myosin VI via SHRImP support a simplified hand-over-hand model. *Biophys. J.* 89:413–17
2. Bartko AP, Dickson RM. 1999. Imaging three-dimensional single molecule orientations. *J. Phys. Chem. B*. 103:11237–41
3. Bartko AP, Dickson RM. 1999. Three-dimensional orientations of polymer-bound single molecules. *J. Phys. Chem. B*. 103:3053–56
4. Bartko AP, Xu K, Dickson RM. 2002. Three-dimensional single molecule rotational diffusion in glassy state polymer films. *Phys. Rev. Lett*. 89:026101
5. Betzig E, Patterson GH, Sougrat R, Lindwasser OW, Olenych S, et al. 2006. Imaging intracellular fluorescent proteins at nanometer resolution. *Science* 313:1642–45
6. Block SM, Goldstein LS, Schnapp BJ. 1990. Bead movement by single kinesin molecules studied with optical tweezers. *Nature* 348:384–85
7. Böhmer M, Enderlein J. 2003. Orientation imaging of single molecules by wide-field epifluorescence microscopy. *J. Opt. Soc. Am. B* 20:554–59
8. Burgess S, Walker M, Wang F, Sellers JR, White HD, et al. 2002. The prepower stroke conformation of myosin V. *J. Cell Biol.* 159:983–91
9. Cheezum MK, Walker WF, Guilford WH. 2001. Quantitative comparison of algorithms for tracking single fluorescent particles. *Biophys. J.* 81:2378–88
10. **Churchman LS, Okten Z, Rock RS, Dawson JF, Spudich JA. 2005. Single molecule high-resolution colocalization of Cy3 and Cy5 attached to macromolecules measures intramolecular distances through time. *Proc. Natl. Acad. Sci. USA* 102:1419–23**
11. **Dahan M, Levi S, Luccardini C, Rostaing P, Riveau B, Triller A. 2003. Diffusion dynamics of glycine receptors revealed by single-quantum dot tracking. *Science* 302:442–45**

10. First demonstration of SHREC, or two-color FIONA.

11. First use of quantum dots for in vivo studies.

12. Dyba M, Hell SW. 2002. Focal spots of size lambda/23 open up far-field fluorescence microscopy at 33 nm axial resolution. *Phys. Rev. Lett*. 88:163901
13. Forkey JN, Quinlan ME, Goldman YE. 2000. Protein structural dynamics by single-molecule fluorescence polarization. *Prog. Biophys. Mol. Biol*. 74:1–35
14. Forkey JN, Quinlan ME, Goldman YE. 2005. Measurement of single macromolecule orientation by total internal reflection fluorescence polarization microscopy. *Biophys. J*. 89:1261–71
15. **Forkey JN, Quinlan ME, Shaw MA, Corrie JE, Goldman YE. 2003. Three-dimensional structural dynamics of myosin V by single-molecule fluorescence polarization. *Nature* 422:399–404**
16. Geerts H, De Brabander M, Nuydens R, Geuens S, Moeremans M, et al. 1987. Nanovid tracking: a new automatic method for the study of mobility in living cells based on colloidal gold and video microscopy. *Biophys. J*. 52:775–82
17. Gelles J, Schnapp BJ, Sheetz MP. 1988. Tracking kinesin-driven movements with nanometre-scale precision. *Nature* 331:450–53
18. **Gordon MP, Ha T, Selvin PR. 2004. Single-molecule high-resolution imaging with photobleaching. *Proc. Natl. Acad. Sci. USA* 101:6462–65**
19. Ha T, Enderle T, Chemla DS, Selvin PR, Weiss S. 1996. Single molecule dynamics studied by polarization modulation. *Phys. Rev. Lett*. 77:3979–82
20. Hofmann M, Eggeling C, Jakobs S, Hell SW. 2005. Breaking the diffraction barrier in fluorescence microscopy at low light intensities by using reversibly photoswitchable proteins. *Proc. Natl. Acad. Sci. USA* 102:17565–69
21. Kinosita K Jr, Itoh H, Ishiwata S, Hirano K, Nishizaka T, Hayakawa T. 1991. Dual-view microscopy with a single camera: real-time imaging of molecular orientations and calcium. *J. Cell Biol*. 115:67–73
22. **Kural C, Kim H, Syed S, Goshima G, Gelfand VI, Selvin PR. 2005. Kinesin and dynein move a peroxisome in vivo: a tug-of-war or coordinated movement? *Science* 308:1469–72**
23. Larson DR, Zipfel WR, Williams RM, Clark SW, Bruchez MP, et al. 2003. Water-soluble quantum dots for multiphoton fluorescence imaging in vivo. *Science* 300:1434–36
24. Mallik R, Carter BC, Lex SA, King SJ, Gross SP. 2004. Cytoplasmic dynein functions as a gear in response to load. *Nature* 427:649–52
25. Michalet X, Pinaud FF, Bentolila LA, Tsay JM, Doose S, et al. 2005. Quantum dots for live cells, in vivo imaging, and diagnostics. *Science* 307:538–44
26. Nan X, Sims PA, Chen P, Xie XS. 2005. Observation of individual microtubule motor steps in living cells with endocytosed quantum dots. *J. Phys. Chem. B* 109:24220–24
27. Ökten Z, Churchman LS, Rock RS, Spudich JA. 2004. Myosin VI walks hand-over-hand along actin. *Nat. Struct. Mol. Biol*. 11(9):884–87
28. Park H, Ramamurthy B, Travaglia M, Safer D, Chen LQ, et al. 2006. Full-length myosin VI dimerizes and moves processively along actin filaments upon monomer clustering. *Mol. Cell* 21:331–36
29. Patra D, Gregor I, Enderlein J. 2004. Image analysis of defocused single-molecule images for three-dimensional molecule orientation studies. *Phys. Chem. A* 108:6836–41
30. Prummer M, Sick B, Hecht B, Wild UP. 2003. Three-dimensional optical polarization tomography of single molecules. *J. Chem. Phys*. 118:9824–29

15. First experiment measuring rotational dynamics at the single-molecule level.

18. Describes measuring small distances using SHRImP.

22. First example of in vivo FIONA with high positional accuracy and temporal resolution.

31. Rasnik I, McKinney SA, Ha T. 2006. Nonblinking and long-lasting single-molecule fluorescence imaging. *Nat. Methods* 3:891–93
32. Reck-Peterson SL, Yildiz A, Carter AP, Gennerich A, Zhang N, Vale RD. 2006. Single-molecule analysis of dynein processivity and stepping behavior. *Cell* 126:335–48
33. Rief M, Rock RS, Mehta AD, Mooseker MS, Cheney RE, Spudich JA. 2000. Myosin-V stepping kinetics: a molecular model for processivity. *Proc. Natl. Acad. Sci. USA* 97:9482–86
34. Rock RS, Rice SE, Wells AL, Purcell TJ, Spudich JA, Sweeney HL. 2001. Myosin VI is a processive motor with a large step size. *Proc. Natl. Acad. Sci. USA* 98:13655–59
35. Sakamoto T, Yildiz A, Selvin PR, Sellers JR. 2005. Step-size is determined by neck length in myosin V. *Biochemistry* 44:16203–10
36. Sheets ED, Lee GM, Simson R, Jacobson K. 1997. Transient confinement of a glycosylphosphatidylinositol-anchored protein in the plasma membrane. *Biochemistry* 36:12449–58
37. Snyder GE, Sakamoto T, Hammer JA 3rd, Sellers J, Selvin PR. 2004. Nanometer localization of single green fluorescent proteins: evidence that myosin V walks hand-over-hand via telemark configuration. *Biophys. J.* 87:1776–83
38. Sosa H, Peterman EJ, Moerner WE, Goldstein LS. 2001. ADP-induced rocking of the kinesin motor domain revealed by single-molecule fluorescence polarization microscopy. *Nat. Struct. Biol.* 8:540–44
39. Syed S, Snyder GE, Franzini-Armstrong C, Selvin PR, Goldman YE. 2006. Adaptability of myosin V studied by simultaneous detection of position and orientation. *EMBO J.* 25:1795–803

40. First characterization of the possible reasons affecting the localization of the dyes.

40. Thompson RE, Larson DR, Webb WW. 2002. Precise nanometer localization analysis for individual fluorescent probes. *Biophys. J.* 82:2775–83
41. Toba S, Watanabe TM, Yamaguchi-Okimoto L, Toyoshima YY, Higuchi H. 2006. Overlapping hand-over-hand mechanism of single molecular motility of cytoplasmic dynein. *Proc. Natl. Acad. Sci. USA* 103:5741–45

42. Defocused imaging is described and it is the first application of DOPI for biological molecules.

42. Toprak E, Enderlein J, Syed S, McKinney SA, Petschek RG, et al. 2006. Defocused orientation and position imaging (DOPI) of myosin V. *Proc. Natl. Acad. Sci. USA* 103:6495–99
43. Valentine MT, Fordyce PM, Krzysiak TC, Gilbert SP, Block SM. 2006. Individual dimers of the mitotic kinesin motor Eg5 step processively and support substantial loads in vitro. *Nat. Cell Biol.* 8:470–76
44. Walker ML, Burgess SA, Sellers JR, Wang F, Hammer JA 3rd, et al. 2000. Two-headed binding of a processive myosin to F-actin. *Nature* 405:804–7
45. Warshaw DM, Kennedy GG, Work SS, Krementsova EB, Beck S, Trybus KM. 2005. Differential labeling of myosin V heads with quantum dots allows direct visualization of hand-over-hand processivity. *Biophys. J.* 88:L30–32
46. Willig K, Kellner R, Medda R, Hein B, Jakobs S, Hell S. 2006. Nanoscale resolution in GFP-based microscopy. *Nat. Methods* 3:721–23
47. Willig KI, Rizzoli SO, Westphal V, Jahn R, Hell SW. 2006. STED microscopy reveals that synaptotagmin remains clustered after synaptic vesicle exocytosis. *Nature* 440:935–39
48. Yasuda R, Noji H, Kinosita K Jr, Motojima F, Yoshida M. 1997. Rotation of the gamma subunit in F1-ATPase; evidence that ATP synthase is a rotary motor enzyme. *J. Bioenerg. Biomembr.* 29:207–9

49. Yildiz A, Forkey JN, McKinney SA, Ha T, Goldman YE, Selvin PR. 2003. Myosin V walks hand-over-hand: single fluorophore imaging with 1.5-nm localization. ***Science*** **300:2061–65**

50. Yildiz A, Park H, Safer D, Yang Z, Chen LQ, et al. 2004. Myosin VI steps via a hand-over-hand mechanism with its lever arm undergoing fluctuations when attached to actin. *J. Biol. Chem.* 279:37223–26

51. Yildiz A, Tomishige M, Vale RD, Selvin PR. 2004. Kinesin walks hand-over-hand. *Science* 303:676–78

49. FIONA is described in detail; the walking mechanism of myosin V is discovered.

Annual Review of Biophysics and Biomolecular Structure

Volume 35, 2006

Contents